Design and Characterization of a Fully 3D Printed Vision-Based Micro-Force Sensor for Microrobotic Applications*

Georges Adam[1], Gwenn Ulliac[2], Cedric Clevy[2], and David J. Cappelleri[1,3]

***Abstract*— Over the years, research and development into micro-force sensing techniques has gained a lot of traction, especially for microrobotic applications, such as micromanipulation and biomedical material characterization studies. Moreover, in recent years, new microfabrication techniques have been developed, such as two-photon polymerization (2PP), which enables fast prototyping, high resolution features, and the utilization of a wide range of materials. In this work, these two fields are combined to realize the first fully 3D printed vision-based micro-force sensor. The sensor exhibits tunable stiffness properties, which are simulated and compared with calibration values for a variety of 2PP printing settings. Lastly, the sensors are used to measure the mechanical properties of fish eggs as a cell analog to showcase the possible applications of the system.**

I. INTRODUCTION

Micromanipulation can be defined as the controlled handling of microstructures ranging in size from a few to hundreds of micrometers, consisting of a very broad and promising field within the microtechnologies world. With the ever growing minituarization demand for electromechanical systems, the necessity of a high precision and robust system to manipulate and assemble such devices has emerged. Furthermore, the growth of the biomedical field and studies of the effects of forces on cells and tissues (mechanobiology) also contributes to an increasing demand for such a system. For these application scenarios, the micromanipulation field emerged, gaining more traction and many systems were developed. In general, micromanipulation systems can be divided into two categories: tethered and untethered. The main difference between these two is related to the accuracy of the system. Untethered systems are dependent on field-driven actuation [1], [2], [3]. Therefore, having precise position control can be challenging. However, tethered systems typically provide more accurate position control through motor actuator feedback and thus more accurate micromanipulation [4], [5]. One drawback of tethered systems is that they can be hard to miniaturize and the size of end-effectors tend to dominate the system field of view, reducing the practical workspace area. Here, work on developing miniaturized micro-force sensing end-effectors for a tethered micromanipulation system is developed to overcome this limitation.

When dealing with manipulation at small scales, surface and contact forces become extremely important and nonintuitive. Therefore, the micromanipulation system's ability to sense its environment is crucial for the development of the field and it enables more complex and accurate applications. While the manipulation of rigid micro-objects does not require micro-force sensing, such capabilities allow for the development of closed-loop systems with much higher accuracy, repeatability, and throughput. Furthermore, the use of micromanipulation systems for biomedical applications require micro-force sensing since the objects being studied (single cells, tissues,

*This work was supported by NSF IIS Award 1763689, NSF CMMI Award 2018570, the FACE Foundation, the Chateaubriand Fellowship program in STEM, and the EIPHI graduate school contract ANR-17-EURE-0002.

[1]Georges Adam and David J. Cappelleri are with the School of Mechanical Engineering, Purdue University, 534 Gates Rd, West Lafayette, IN, USA. [adamg, dcappell]@purdue.edu

[2]Cedric Clevy and Gwenn Ulliac are with FEMTO-ST Institute, Univ. Bourgogne Franche-Comte, UMR CNRS 6174, Besancon,. cclevy@univ-fcomte.fr, gwenn.ulliac@femto-st.fr

[3]David J. Cappelleri is also with the Weldon School of Biomedical Engineering, Purdue University, 206 S Martin Jischke Dr., West Lafayette, IN, USA.

etc.) are fragile and can be easily damaged if too high manipulation forces are applied. Lastly, many applications also require the input of specific micro-forces in order to study the biological response of such forces, such as the field of mechanobiology [6], [7], [8], and for mechanical characterization studies [9], [10].

In the past, many micro-force sensing techniques and modalities for micromanipulation have been explored, such as piezoelectric/piezoresistive [11], [12], [13], capacitive-based [14], AFM-based methods [15], [16], vision-based [17], [18], [19], strain gauges [20], [21], among others. For this study, a vision-based micro-force sensor is developed for its simplicity in design that can be scaled down and directly 3D printed with tailored stiffness values. It also overcomes many of the drawbacks of the other types of micro-force sensors, such as high costs and difficult integration into micromanipulation systems (AFM-based sensors), non-linear sensor requiring multiple calibrations (strain gauges), temperature and humidity sensitivity (capacitive-based sensors). Vision-based micro-force sensors are purely mechanical, compliant structures with calibrated stiffness values, thus they do not require any electronics or signal conditioning. For the micro-force ranges for which they are used, they can function under the Hooke's law principle so that when a force is applied to the end of the sensor, the measured deflection of the structure is directly correlated to the applied force.

Traditionally, vision-based micro-force sensors have been fabricated using standard 2D micro-fabrication techniques, such as photolithography and etching, micromolding, or other methods to pattern a soft material [17], [22], [23]. However, with the development of fast lasers (femtosecond repetition rate), new 3D fabrication systems based on Two-Photon Polymerization (2PP or TPP) have been developed, enabling fast prototyping, with complex 3D geometries and a multitude of material options (including soft resins and responsive materials), while simultaneously achieving sub-micrometer resolution and structures ranging in size from a few microns to a few millimeters. This powerful micro-fabrication technique requires a study of the optimal printing settings and geometries for specific designs. Oftentimes, a parametric sweep is required to print complex 3D shapes, such as undercuts and small structures. The attachment to the substrate must also be considered: large contact areas with the substrate can result in difficulties releasing the part post-print, and low contact areas can result in premature release during the printing process. Additionally, the mechanical properties of the resultant structures are often unknown due to the high number of print settings and inherent viscoelastic behavior presented by certain resins, especially softer ones. In this paper, the first fully 3D printed vision-based micro-force sensor is developed and characterized. The design is tuned for the 2PP printing capabilities and available materials. The simulated tunable sensor stiffness are compared to the calibrated values with the printed designs. Subsequently, this sensor is utilized to characterize the mechanical properties of fish eggs, as cell analogs.

II. SENSOR DESIGN AND FABRICATION

A. Design

A vision-based force sensor is a device that consists of a pre-calibrated compliant structure of known stiffness (k) and a vision system that is able to track deflections (Δx). When a force is applied to the sensor, a measurable deflection can be tracked and the principle of Hooke's law is used to compute the applied force ($F = k \cdot \Delta x$). In the past, vision-based micro-force sensors were created using standard microfabrication techniques, such as multiple photolithography steps

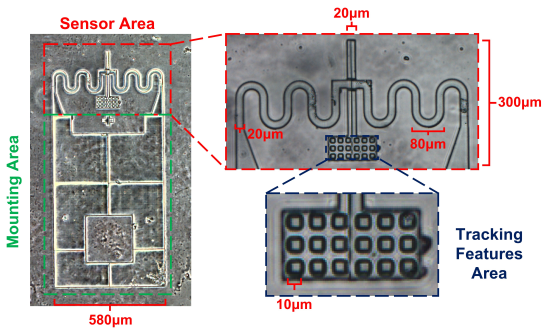

Fig. 1. Overview of the sensor design with critical dimensions annotated. The lines running through the design correspond to the stitching of the 400 μm blocks. The rectangular pattern on the bottom right part of the figure represent the computer vision tracking markers.

followed by deep etching and polymer deposition. These multi-step processes require a lot of time and are limited to fabricating monolithic 2D structures. Furthermore, they require multiple masks to create the geometry patterns, making it difficult and time-consuming to iterate on the design, if needed. Additionally, their geometric complexity and material also limited the scaling down of the critical dimensions of the compliant structure in the sensor. Conversely, using 2PP fabrication, complex 3D shapes are attainable for a wide range of materials. The printing resolution can reach the range of hundreds of nanometers and different designs can be prototyped with just changes to a CAD file. Also, the size of the structures to be printed can easily be scaled down in size.

Taking inspiration from our previous design of a vision-based micro-force sensor (μVBFS) [18], [19], a similar sensor design was fabricated here using the 2PP principles, taking advantage of the capabilities mentioned earlier. Figure 1 shows a schematic of the overall sensor design with its rigid body and compliant spring-like structure, along with critical dimensions. With the advantages of the 2PP fabrication method, different designs can be quickly printed and tested, including different end-effectors or the use of different print settings to create sensors with different mechanical properties. Furthermore, squared markers were added to the back part of the compliant structure. They are used to make it easier for the computer vision algorithms to locate and track the deflections of the compliant spring, thus resulting in a more robust and accurate micro-force sensor. These markers are shown in the tracking feature area region of Fig. 1. Lastly, due to the easy prototyping provided by 2PP fabrication, a mounting hole has been added to the back of the design for easier assembly onto a micromanipulator probe. This is shown in the mounting area of Fig. 1.

B. *Fabrication*

Two-photon polymerization, referred to here as 2PP, is a recent innovation in the micro/nano-fabrication field that allows the 3D printing of small scale structures with high accuracy and the ability to produce complex 3D geometries. Moreover, it has a high range of possible fabrication materials, which enables the development of tailored structures with different mechanical properties and even the fabrication of active structures, commonly called 4D printing. This method is based on the two-photon absorption principle, in which an atom is able to absorb two photons and go to a higher energy state in which the radicals are locally excited and they crosslink within the photoresin causing polymerization. This process is governed by a very brief virtual state, thus the need to use lasers with high repetition rates (around the femtosecond range). Additionally, the crosslinking process decays in the order of distance squared, enabling the polymerization of just a small region, resulting in high resolution fabrication. In this case, the Nanoscribe Photonic Professional GT2 printer (Nanoscribe GmbH & Co.) which uses a Near-Infrared (NIR) femtosecond laser was utilized to fabricate the first fully 3D printed vision-based micro-force sensor.

In this manuscript, a few different fabrication settings are used to create slightly different sensors and compared the overall stiffness of each design. All of them are fabricated using the IP-S photoresin (Nanoscribe GGmbH & Co.) and the standard fabrication recipe (laser power and scan speed combinations). Three types of designs in total were studied. For each device printed, the laser power and scan speed were kept constant at 100% and 100,000 μm/s (or 100 mm/s), respectively, since these values were shown to work well with IP-S prints. The main difference between each type of sensor is the fill settings on the compliant spring section for each design. By just changing the fill setting, the three different types of sensors can be produced from the same CAD file. The complaint springs either have solid cross-sections (Type 1), triangular scaffolding (Type 2), or hollow cross-sections (Type 3), as shown in Fig. 2 (a-c). One of the major issues with 2PP fabrication is the release of fragile structures from the substrate without breaking them. To solve this issue, the compliant structure was designed with a trapezoidal base, which effectively reduces the contact area with the substrate by half, as shown in Fig. 2(d).

Using these settings, the sensors were fabricated using the 25x (NA 0.8) lens in a Dip-in Laser Lithography (DiLL) configuration with ITO-coated sodalime glass substrates (indium-tin oxide). These substrates are used with this configuration to increase the adhesion forces to keep the structure from being released prematurely. Using this configuration, the highest resolution attainable is in the order of 2 μm with printing field of 400 μm $\times$ 400 μm. Since the overall structure is larger than the printing field, the sensor is constructed by splitting the design into smaller blocks that are stitched together. Figure 1 shows the lines where the sensor is stitched together to create the the mounting area region and connect it to the sensor area region of the device.

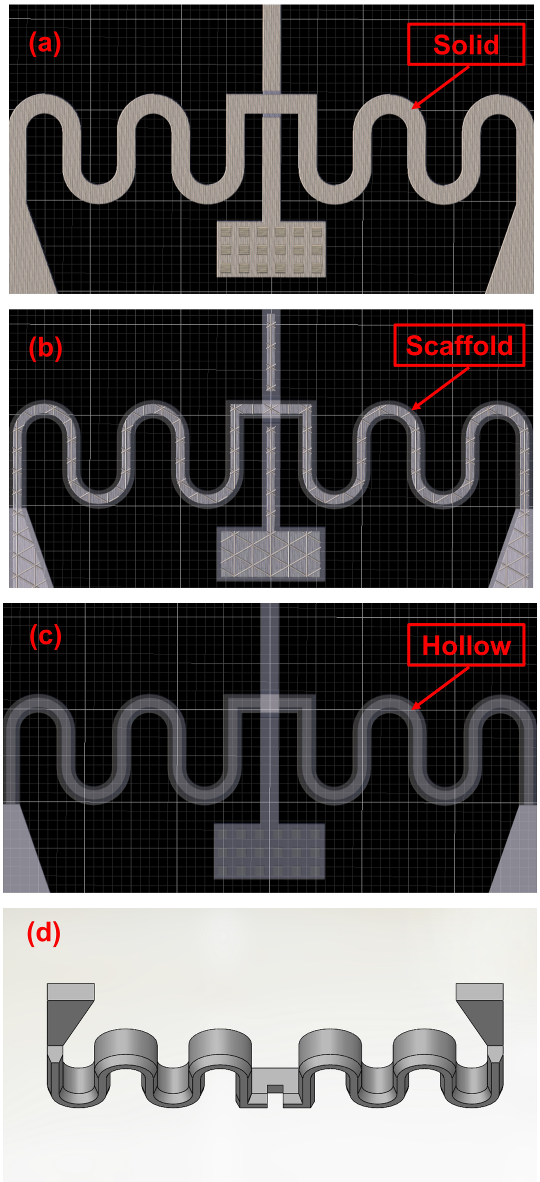

Fig. 2. Different fill settings and complex 3D geometries made possible by 2PP fabrications. (a) solid spring (Type 1), (b) triangular scaffold spring (Type 2), (c) hollow spring (Type 3), and (d) trapezoidal spring base for easier substrate release.

III. SIMULATIONS & CHARACTERIZATION

A. FEA Simulations

In order to accurately sense micro-forces, the spring structure of the device must be designed with low stiffness in each of the planar (XY) 2D sensing dimensions. This stiffness is a function of the spring geometry and material property of the structure itself. While the 2PP system produces a very accurate replication of the designed geometry in the produced prototypes, the material properties given by the resin's manufacturer only apply to the standard print settings. Thus, any deviation from these print settings may result in different material properties and thus different device stiffness.

Using the material properties provided by the resin's manufacturer for IP-S (E = 5.11 GPa, ν = 0.3), a finite element analysis (FEA) of the Type 1 design spring structure was compiled. For the simulations, the sensor body was fixed and a load was applied directly to the end-effector. The simulation results are shown in Fig. 3. The slope of the linear fit from the force versus displacement plot corresponds to the sensor stiffness in the direction (Y-axis) of the applied force. For this base design with standard material properties, the stiffness is k_y = 24.78 N/m.

The sensing resolution of a vision-based sensor is given by the directional stiffness of the compliant structure and the spacial resolution of the camera system utilized, i.e., the actual distance each pixel represents in the camera frame. Therefore, there is a trade-off between the overall size of the workspace and the force sensing resolution of the system. For the sensor calibration, a higher resolution camera is used to achieve the most

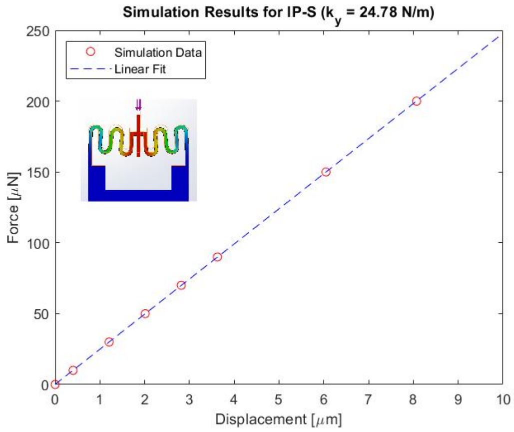

Fig. 3. FEA analysis of the stiffness of the spring-like compliant structure of the sensor. Plot shows the data acquired from the simulation and the linear fit to compute the stiffness.

accurate characterization, however, for practical uses, a camera with a larger workspace view and thus smaller spacial resolution is used.

B. Mechanical Characterization

In order to compute the true stiffness of the different printed sensors, an experimental setup with a micromanipulator, camera, and mount was developed, as shown in Fig. 4. Here, a reference force sensor (Femto Tools FT-S100) is pushed against the printed sensor prototypes with known displacements given by the micromanipulation system (MP-225, Sutter Instruments). This system is being utilized with steps of 1 μm per step. Therefore, by slowly increasing the displacement, a force versus displacement plot can be presented for the printed sensor, thus calibrating its stiffness. Figure 5(a) shows the loading profile (force over time), from where the data is extracted to create the force versus displacement plot, as shown in Fig.5(b), for a Type 1 prototype. This is done for both the loading and unloading portion of the characterization, resulting in two lines that should theoretically have the same stiffness. This same process is repeated 3 times using the same sensor to achieve an accurate measure of its stiffness.

From the loading profile shown in Fig. 5(a), it can be seen that the forces change slightly as time goes on for the same micromanipulator deflection. Some of the noise can be attributed to the reference sensor's sensitivity, which is highly affected by any vibrations in the room, including the motion of the stepper motors in the micromanipulator system. Furthermore, the changes in force can also be attributed to the viscoelastic behavior of the printing material. According to its datasheet, IP-S has a storage modulus of 5.33 GPa and a loss modulus of 0.26 GPa, resulting in a small loss tangent value, which indicates almost no phase lag between stress and strain. As expected, the behavior of the sensor during the calibration follows that of a material with small viscoelastic behavior.

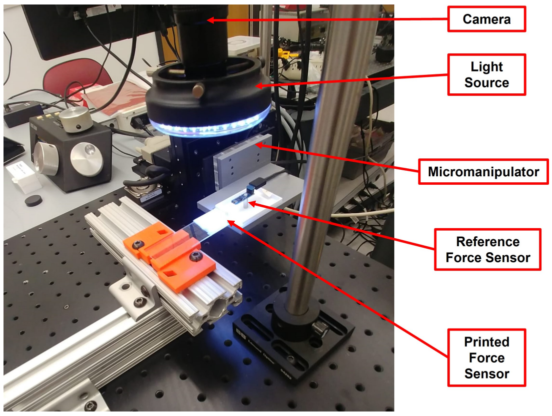

Fig. 4. Calibration setup using a micromanipulator (MP-225, Sutter Instruments), camera system (Flea3, PointGrey), and reference force sensor (FT-S100, Femto Tools).

Since 2PP is a relatively new fabrication technique, there are many questions that remain unanswered regarding its performance and expected results. Firstly, how does the material properties of the printed sensors relate to the simulation values obtained by using the nominal material properties of the resin? Additionally, how do these results compare when two sensors are printed using different 2PP machines? To answer these questions, 4 different sensors were calibrated using the experimental setup described above and the results compared, as shown in Table I. Each sensor was calibrated 3 times for more accurate results. Note: sensors Type 1a and Type 1b are both made out of solid IP-S, but Type 1a was made using a GT+ system in France (FEMTO-ST) and Type 1b was fabricated using a GT2 system in the United States (Purdue University). Type 2 and Type 3 sensors were fabricated with the triangular mesh and hollow spring deigns, respectively, as

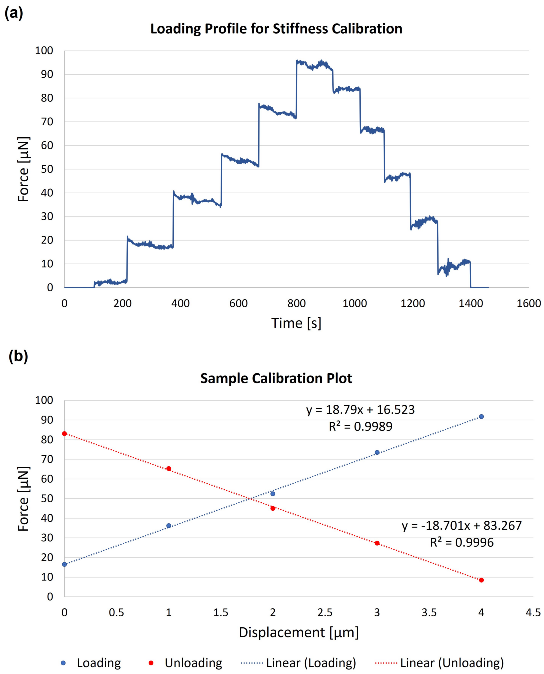

Fig. 5. (a) Loading and unloading profile for the stiffness characterization of the Type 1b μVBFS. (b) Sample calibration plot extracting the force values from the loading profile and deflections from the micromanipulator motion. The slope of the two lines indicate the stiffness results when analyzing the loading and unloading of the force sensor.

previously described.

Based on the calibration results, it is clear that the stiffness of the Type 1 solid sensors match regardless of the equipment that was used. Interestingly enough, the Type 2 design with the triangular scaffolding on the inside has the same stiffness as the solid Type 1 IP-S designs. It seems that the amount of trusses on the inside of the structure make up for the lack of material and keep the same overall stiffness. This can be used as a more optimal printing parameter for the sensor, since it not only has the same stiffness, but also prints the structure 3 times as fast, resulting in higher throughput without compromising the structural integrity of the design. As expected, the Type 3 hollow design has the smallest stiffness of all the sensors fabricated and tested here. This shows that the printing properties can have a large impact on the resultant stiffness, and along with geometry changes, can lead to specifically

TABLE I

STIFFNESS CALIBRATION FOR DIFFERENT 2PP PRINTED SENSOR TYPES ALONG WITH STANDARD DEVIATION (ST. DEV.)

Sensor	Description	Stiffness (N/m)	St. Dev.
Type 1a	Solid IP-S made in France	18.23	0.18
Type 1b	Solid IP-S made in the US	18.56	0.81
Type 2	IP-S w/ triangular scaffold	18.03	0.94
Type 3	Hollow IP-S	7.27	0.92

tailored sensors based on the target application. Comparing the calibrated stiffness of the solid sensors (Type 1a and 1b) to the simulations results in Fig. 3, they are in the same order of magnitude, but not exactly the same. As mentioned before, the discrepancy in the values can be caused by many factors since the stiffness is highly dependent on printing parameters. In general, simulations are useful to obtain an approximate value for the stiffness, however each sensor must still be calibrated individually before use for higher accuracy in the force sensing.

IV. FORCE-SENSING APPLICATIONS

One of the many possible applications for the sensor developed in this work is the characterization of the mechanical properties of biological media, such as cells, tissues, proteins, etc. To showcase the μVBFS capabilities, the sensor was utilized to measure the stiffness of approximately 2 mm diameter salmon eggs, used here as larger scale cell analog. For this experiment, the force sensor was attached to the end of a micromanipulator probe [19], [18] so it can be precisely guided to the egg outer wall and then perform controlled force exertion for the characterization. The egg itself is secured to a glass slide substrate to prevent it from sliding and making sure all the applied force translates into outer wall deflection. Then, all the components are mounted under a camera system to record the relative deflections of the μVBFS and the egg's outer wall.

This system can be modelled as two springs in series with stiffness k_{sensor} and k_{egg} for the force sensor and salmon egg, respectively. Once the sensor is pushed against the egg using the

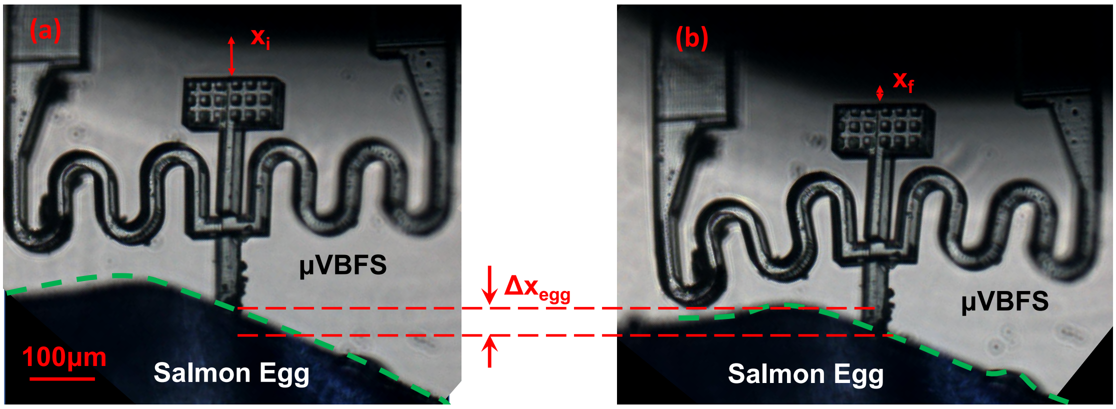

Fig. 6. Camera view of the stiffness characterization of a salmon egg (outlined in green) using the μVBFS. (a) shows the initial position (undeflected state) and (b) shows the final position (under load).

micromanipulation system, the same force, F, is applied to the sensor and egg. Therefore, by using Hooke's law, we have:

$$F = k_{sensor} \cdot \Delta x_{sensor} = k_{egg} \cdot \Delta x_{egg} \quad (1)$$

where Δx_{sensor} and Δx_egg are the relative displacement of the sensor and the egg, respectively. By reorganizing the equation, it is possible to solve for the stiffness of the egg, as shown in Eq. 2:

$$k_{egg} = \frac{k_{sensor} \cdot \Delta x_{sensor}}{\Delta x_{egg}} \quad (2)$$

Here, the stiffness of the sensor is known based on its calibration, and the relative displacements are computed using the vision system. Figure 6(a) shows the initial position of the sensor and Fig. 6(b) the system under load. By comparing the distance of the spring markers to the micromanipulator probe body, the overall displacement of the compliant structure can be computed. Similarly, the position of the egg wall can be compared between the initial and final states to obtain its relative displacement. Using this method described above, the stiffness of the salmon egg was computed to be 20.55 N/m $\pm$ 1.92. This result comes from averaging the computed stiffness at different deflection values after repeatedly performing pushes against the egg outer wall. Furthermore, the sensor was able to puncture the egg's wall and the puncture force recorded to be approximately 725 μN.

V. CONCLUSIONS

In this paper, the design and characterization of the first fully 3D printed vision-based micro-force sensor is presented. The sensor is completely fabricated using 2PP techniques which provides a high resolution, fast, and versatile microfabrication method that is also able to create complex 3D shapes at small scales. These fabricated sensors were characterized and compared to simulations based on the nominal material properties of the photoresin used. It is shown that the printing settings greatly affects the overall stiffness of the fabricated sensor, but the results remain consistent for the same print settings. In order to showcase the capabilities and possible applications of such sensor, it was used to mechanically characterize salmon egg cell analogs.

ACKNOWLEDGMENT

The authors acknowledge the facility access at FEMTO-ST Mimento cleanroom and Purdue University's Birck Nanotechnology Center, and technical assistance from Dr. Joël Agnus and Patrick Rougeot.

REFERENCES

[1] Z. Chen, X. Liu, M. Kojima, Q. Huang, and T. Arai, "Advances in micromanipulation actuated by vibration-induced acousticwaves and streaming flow," p. 1260, 2 2020.

[2] S. Zhang, E. Y. Scott, J. Singh, Y. Chen, Y. Zhang, M. Elsayed, M. Dean Chamberlain, N. Shakiba, K. Adams, S. Yu, C. M. Morshead, P. W. Zandstra, and A. R. Wheeler, "The optoelectronic microrobot: A versatile toolbox for micromanipulation," *Proceedings of the National Academy of Sciences of the United States of America*, vol. 116, no. 30, pp. 14 823–14 828, 7 2019.

[3] M. Zhu, K. Zhang, H. Tao, S. Hopyan, and Y. Sun, "Magnetic Micromanipulation for In Vivo Measurement of Stiffness Heterogeneity and Anisotropy in the Mouse Mandibular Arch," 2020.

[4] J. A. Seon, R. Dahmouche, and M. Gauthier, "Enhance In-Hand Dexterous Micromanipulation by Exploiting Adhesion Forces," *IEEE Transactions on Robotics*, vol. 34, no. 1, pp. 113–125, 2 2018.

[5] B. Brazey, R. Dahmouche, J. A. Seon, and M. Gauthier, "Experimental validation of in-hand planar orientation and translation in microscale," *Intelligent Service Robotics*, vol. 9, no. 2, pp. 101–112, 2016.

[6] M. Krieg, G. Fläschner, D. Alsteens, B. M. Gaub, W. H. Roos, G. J. Wuite, H. E. Gaub, C. Gerber, Y. F. Dufrêne, and D. J. Müller, "Atomic force microscopy-based mechanobiology," *Nature Reviews Physics 2018 1:1*, vol. 1, no. 1, pp. 41–57, 2018.

[7] B. Özkale, M. S. Sakar, and D. J. Mooney, "Active biomaterials for mechanobiology," *Biomaterials*, vol. 267, p. 120497, 1 2021.

[8] S. Kim, M. Uroz, J. L. Bays, and C. S. Chen, "Harnessing Mechanobiology for Tissue Engineering," *Developmental Cell*, vol. 56, no. 2, pp. 180–191, 1 2021.

[9] X. Wang, J. Law, M. Luo, Z. Gong, J. Yu, W. Tang, Z. Zhang, X. Mei, Z. Huang, L. You, and Y. Sun, "Magnetic Measurement and Stimulation of Cellular and Intracellular Structures," *ACS nano*, vol. 14, no. 4, pp. 3805–3821, 2020.

[10] G. Adam, M. Hakim, L. Solorio, and D. J. Cappelleri, "Stiffness Characterization and Micromanipulation for Biomedical Applications using the Vision-based Force-Sensing Magnetic Mobile Microrobot," in *Proceedings of MARSS 2020: International Conference on Manipulation, Automation, and Robotics at Small Scales*. IEEE, 7 2020.

[11] T. Abondance, T. Abondance, K. Jayaram, N. T. Jafferis, J. Shum, and R. J. Wood, "Piezoelectric Grippers for Mobile Micromanipulation," *IEEE Robotics and Automation Letters*, vol. 5, no. 3, pp. 4407–4414, 7 2020.

[12] G. Wang and Q. Xu, "Design and Precision Position/Force Control of a Piezo-Driven Microinjection System," *IEEE/ASME Transactions on Mechatronics*, vol. 22, no. 4, pp. 1744–1754, 8 2017.

[13] B. Tiwari, M. Billot, C. Clévy, J. Agnus, E. Piat, and P. Lutz, "A Two-Axis Piezoresistive Force Sensing Tool for Microgripping," *Sensors 2021, Vol. 21, Page 6059*, vol. 21, no. 18, p. 6059, 9 2021.

[14] X. Sun, W. Chen, W. Chen, S. Qi, W. Li, C. Hu, and J. Tao, "Design and analysis of a large-range precision micromanipulator," *Smart Materials and Structures*, vol. 28, no. 11, p. 115031, 10 2019.

[15] S. Guo, X. Zhu, D. Jańczewski, S. Siew Chen Lee, T. He, S. Lay Ming Teo, and G. Julius Vancso, "Measuring protein isoelectric points by AFM-based force spectroscopy using trace amounts of sample," *Nature Nanotechnology*, vol. 11, 2016.

[16] M. Annadhasan, D. P. Karothu, R. Chinnasamy, L. Catalano, E. Ahmed, S. Ghosh, P. Naumov, and R. Chandrasekar, "Micromanipulation of Mechanically Compliant Organic Single[U+2010]Crystal Optical Microwaveguides," *Angewandte Chemie*, vol. 132, no. 33, pp. 13 925–13 934, 8 2020.

[17] M. Guix, J. Wang, Z. An, G. Adam, and D. J. Cappelleri, "Real-Time Force-Feedback Micromanipulation Using Mobile Microrobots With Colored Fiducials," *IEEE Robotics and Automation Letters*, 2018.

[18] G. Adam and D. J. Cappelleri, "Towards a real-time 3D vision-based micro-force sensing probe," *Journal of Micro-Bio Robotics*, 2020.

[19] G. Adam, S. Chidambaram, S. S. Reddy, K. Ramani, and D. J. Cappelleri, "Towards a Comprehensive and Robust Micromanipulation System with Force-Sensing and VR Capabilities," *Micromachines 2021, Vol. 12, Page 784*, vol. 12, no. 7, p. 784, 6 2021.

[20] J. Qu, Q. Wu, T. Clancy, Q. Fan, X. Wang, and X. Liu, "3D-Printed Strain-Gauge Micro Force Sensors," *IEEE Sensors Journal*, vol. 20, no. 13, pp. 6971–6978, 7 2020.

[21] S. Noveanu, I. A. Ivan, D. C. Noveanu, C. Rusu, and D. Lates, "SiMFlex Micromanipulation Cell with Modular Structure," *Applied Sciences 2020, Vol. 10, Page 2861*, vol. 10, no. 8, p. 2861, 4 2020.

[22] V. Guelpa, J.-S. Prax, Y. Vitry, O. Lehmann, S. Dehaeck, P. Sandoz, C. Clevy, N. Le Fort-Piat, P. Lambert, and G. J. Laurent, "3D-printed vision-based micro-force sensor dedicated to in situ SEM measurements," in *2017 IEEE International Conference on Advanced Intelligent Mechatronics (AIM)*. IEEE, 7 2017, pp. 424–429.

[23] C. Bi, E. E. Niedert, G. Adam, E. Lambert, L. Solorio, C. J. Goergen, and D. J. Cappelleri, "Tumbling Magnetic Microrobots for Biomedical Applications," in *2019 International Conference on Manipulation, Automation and Robotics at Small Scales (MARSS)*. IEEE, 7 2019, pp. 1–6.